Coupled lateral and vertical electron dynamics in semiconductor superlattices

A. Amann* and E. Schöll

Institut für Theoretische Physik, Technische Universität Berlin, Hardenbergstraße 36, 10623 Berlin, Germany

(Received 7 July 2005; revised manuscript received 26 August 2005; published 17 October 2005)

We develop a theoretical description for a weakly coupled semiconductor superlattice which allows for laterally inhomogeneous charge distributions within one well. We use this model to study the dynamical stability of mixed initial states in which different regions of the superlattice are associated with the different branches in the multistable current-voltage characteristic. It is found that mixed states can indeed exist for a long time; their stability, however, depends very sensitively on the applied external voltage.

I. INTRODUCTION

Since the pioneering work by Esaki and Tsu[1] in the 1970s, vertical electron transport in semiconductor superlattices has been studied extensively. It was demonstrated that the negative differential conductivity in such devices can lead to the formation of field domains giving rise to a variety of interesting phenomena. Examples are a static sawtooth-like current-voltage characteristic,[2–5] self-sustained periodic,[6–10] or chaotic[11–13] current oscillations. For reviews of the relevant theory see Refs. 14–17.

In previous theoretical work it has generally been assumed that inhomogeneities in the electron concentration occur in the vertical (z) direction between different quantum wells only, while each individual well is supposed to be homogeneously charged. While this approximation may be justified if the lateral charge relaxation within one well is very efficient, it is obvious that for superlattices with large lateral extensions, the charge distribution within a quantum well can in principle be nonuniform. For example, switching between different branches of the multistable current-voltage characteristic and domain boundary relocation[18,19] may not occur uniformly. Therefore, it is the purpose of the present work to extend the existing theory to include such lateral inhomogeneities and point out some of the qualitatively different features arising from this additional degrees of freedom.

After introducing the dynamical equations for the laterally extended system in Sec. II, we will describe a practical method for their solution in Sec. III. We will then apply this method in Sec. IV to study the consequences of the lateral degrees of freedom for a superlattice in the regime of stationary field domains, i.e., without self-sustained oscillations. In particular, we will consider the evolution of an initial state, which corresponds to a mixture of different branches in the multistable current density vs voltage characteristic. We will show that the stability of such a state depends sensitively upon the applied voltage, which changes the degree of stability of the individual branches of the multistable characteristic. As a second example, we will study the relaxation of a state prepared with an electron accumulation and depletion front in the same quantum well.

II. DYNAMICAL EQUATIONS

We consider the dynamics of electrons in a n-doped semiconductor superlattice with N quantum wells. The external voltage drop U is applied in the z direction, i.e., perpendicularly to the quantum well layers. On a semiclassical level, the electrons can be assumed to be localized within one quantum well. If we further assume that the electrons are in local equilibrium, the internal state of the superlattice can be described in terms of the two-dimensional charge densities $n_m(x,y,t)$, which in addition to the well index $m \in \{1,\dots,N\}$ also depend on the in-plane coordinates, $x \in [0,L_x]$ and $y \in [0,L_y]$, where L_x and L_y are the lateral extensions of the superlattice in x and y direction, respectively.

The usual continuity equation can then be written in the form

$$e\dot{n}_m(x,y,t) = j_{m-1\to m}^{\parallel} - j_{m\to m+1}^{\parallel} - \boldsymbol{\nabla}_\perp \mathbf{j}_m^\perp \qquad (1)$$

with

$$\boldsymbol{\nabla}_\perp = \mathbf{e}_x \frac{\partial}{\partial x} + \mathbf{e}_y \frac{\partial}{\partial y}, \qquad (2)$$

and the vertical current density in z direction $j_{m\to m+1}^{\parallel}(x,y)$ (units: $[\text{A/m}^2]$), and the lateral two-dimensional current density $\mathbf{j}_m^\perp(x,y)$ (units: $[\text{A/m}]$). The electron charge is $e < 0$.

In the conventional sequential tunneling model without lateral degrees of freedom, the well-to-well current density $j_{m\to m+1}(F_m, n_m, n_{m+1})$, which depends on the electron densities n_m and n_{m+1} of the involved wells and the electric field F_m in the corresponding barrier, is conveniently calculated using Wannier states without any reference to global properties of the superlattice.[15] Therefore, it is reasonable to assume that the local vertical current can be expressed as

$$j_{m\to m+1}^{\parallel}(x,y) = j_{m\to m+1}[F_m^{\parallel}(x,y), n_m(x,y), n_{m+1}(x,y)], \quad (3)$$

where $F_m^{\parallel}(x,y)$ is the local electric field in z direction across the barrier with index m. In other words, we assume that the theory leading to $j_{m\to m+1}$ is still valid locally and take the explicit form of $j_{m\to m+1}$ from a previous work on the sequential tunneling theory.[15] The current densities at the emitter and the collector contact are modeled by Ohmic boundary conditions $j_{0\to 1}^{\parallel} = \sigma F_0^{\parallel}$, $j_{N\to N+1}^{\parallel} = \sigma F_N^{\parallel} n_N/N_D$ with contact conductivity σ, respectively.

In addition to the vertical current, we also have to consider a lateral two-dimensional in-plane current density $\mathbf{j}_m^\perp$ (units: $[\text{A/m}]$). This lateral current can quite generally be written as the sum of a drift term and a diffusion term

$$\mathbf{j}_m^\perp(x,y) = -e\mu n_m \mathbf{F}_m^\perp - eD_0\mathbf{\nabla}_\perp n_m, \tag{4}$$

characterized by the mobility μ and the diffusion coefficient D_0, respectively. Here $\mathbf{F}_m^\perp(x,y)$ is the in-plane component of the electric field in well m at (x,y), whose calculation will be considered in more detail in Sec. III. μ and D_0 are connected by a generalized form of the Einstein relation[20,21]

$$D_0(n_m) = \frac{n_m}{-e\rho_0(1-\exp[-n_m/(\rho_0 k_B T)])}\mu, \tag{5}$$

with $\rho_0 = m/(\pi\hbar^2)$. Note that the mobility μ can in principle also depend on n and that (5) can only be derived for the equilibrium case. In the following, we make the assumptions that μ is fixed (for GaAs, we assume $\mu \approx 10$ m^2/Vs) and that (5) is still valid in the nonequilibrium case. Then we may rewrite (4) as

$$\mathbf{j}_m^\perp(x,y) = -e\mu n_m\left[\mathbf{F}_m^\perp - \frac{\mathbf{\nabla}_\perp n_m}{e\rho_0(1-e^{-n_m/\rho_0 k_B T})}\right]. \tag{6}$$

III. THE POISSON EQUATION

In order to solve the dynamical equation (1) with the current densities given by Eqs. (3) and (4), we need to calculate the local electric fields $F_m^\parallel$ and $\mathbf{F}_m^\perp$. From elementary electrodynamics, it follows that they must obey the following semidiscrete version of Gauss's law

$$F_m^\parallel - F_{m-1}^\parallel + d\mathbf{\nabla}_\perp\mathbf{F}_m^\perp = \frac{e}{\epsilon_r\epsilon_0}(n_m - N_D), \tag{7}$$

where d is the period of the superlattice, ϵ_r and ϵ_0 are the relative and absolute permittivities, and N_D is the two-dimensional doping density. Additionally, we require the boundary conditions

$$U = -\sum_{m=0}^{N} F_m^\parallel(x,y)d \quad \text{for } x \in [0,L_x], \quad y \in [0,L_y], \tag{8}$$

$$\mathbf{F}_m^\perp(0,y) = \mathbf{F}_m^\perp(L_x,y) = \mathbf{F}_m^\perp(x,0) = \mathbf{F}_m^\perp(x,L_y) = 0. \tag{9}$$

For the integration of (1), it is necessary to solve (7) efficiently with respect to the electric fields $\mathbf{F}_m^\perp$ and $F_m^\parallel$. This amounts to the solution of the semidiscrete Poisson equation for the potential $\varphi_m(x,y)$ of the form

$$\Delta\varphi_m(x,y) = (\Delta_\perp + \Delta_\parallel)\varphi_m(x,y) = -\frac{e}{d\epsilon_r\epsilon_0}(n_m - N_D) \tag{10}$$

with

$$\Delta_\perp\varphi_m(x,y) = \left(\frac{\partial^2}{\partial x^2} + \frac{\partial^2}{\partial y^2}\right)\varphi_m(x,y), \tag{11}$$

$$\Delta_\parallel\varphi_m(x,y) = \frac{\varphi_{m-1}(x,y) - 2\varphi_m(x,y) + \varphi_{m+1}(x,y)}{d^2}. \tag{12}$$

A straightforward way for obtaining the potential φ_m from (10) would be to calculate the inverse capacitance matrix

given by the operator Δ^{-1} explicitly. If M is the number of discretization points in the (x,y) plane, this matrix has, however, $(NM)^2$ elements, and we have to perform $O(N^2M^2)$ operations at every integration time step.

In search of a more efficient algorithm, we compare the contributions from $\Delta_\perp\varphi_m$ and $\Delta_\parallel\varphi_m$ in (10). In Ref. 21, the mean free path of the degenerate electrons in the well was estimated as $l_m \approx 0.3$ μm, and we may expect that typical structures in the lateral direction vary on a length scale which is even larger. Indeed it was found by numerical simulation of a single-well double barrier resonant tunneling (DBRT) model that lateral structures typically occur on the length scale of about $l_t = 10$ μm.[22–24] On the other hand, the variations of the potential in the vertical direction z is of the order of the superlattice period $d \approx 10$ nm. We may, therefore, conclude that

$$\Delta_\perp\varphi_m \sim (l_t)^{-2} \ll \Delta_\parallel\varphi_m \sim d^{-2}. \tag{13}$$

This allows us to invert the Laplace operator by the use of a perturbation expansion of the form,

$$\Delta^{-1} = (\Delta_\perp + \Delta_\parallel)^{-1} = (1 + \Delta_\parallel^{-1}\Delta_\perp)^{-1}\Delta_\parallel^{-1} \tag{14}$$

$$\approx (1 - \Delta_\parallel^{-1}\Delta_\perp + \dots)\Delta_\parallel^{-1} = \Delta_\parallel^{-1} - \Delta_\parallel^{-2}\Delta_\perp + \cdots. \tag{15}$$

In the last step, we used the fact that $\Delta_\perp$ and $\Delta_\parallel$ commute. Applying (14) to (10) then yields

$$\varphi_m(x,y) = \varphi_m^0(x,y) + \varphi_m^1(x,y) + \cdots, \tag{16}$$

$$\varphi_m^0(x,y) = -\frac{e}{d\epsilon_r\epsilon_0}\Delta_\parallel^{-1}(n_m - N_D), \tag{17}$$

$$\varphi_m^1(x,y) = +\frac{e}{d\epsilon_r\epsilon_0}\Delta_\parallel^{-2}\Delta_\perp n_m. \tag{18}$$

The advantage of such a solution for (10) lies in the fact that it can be calculated very efficiently. $\varphi_m^0(x,y)$ is evaluated by shooting with

$$\widetilde{\varphi}_0^0(x,y) = \widetilde{\varphi}_1^0(x,y) = 0, \tag{19}$$

$$\widetilde{\varphi}_{m+1}^0(x,y) = 2\widetilde{\varphi}_m^0 - \widetilde{\varphi}_{m-1}^0 - \frac{ed}{\epsilon_r\epsilon_0}(n_m - N_D) \tag{20}$$

and then taking into account the corrections from the boundary conditions by

$$\varphi_m^0(x,y) = \widetilde{\varphi}_m^0 + (U - \widetilde{\varphi}_{N+1}^0)\frac{m}{N+1} \quad \text{for } m = 1\dots N+1. \tag{21}$$

The algorithm described by (20) and (21) needs only $O(NM)$ operations.

Also the matrix multiplication $\Delta_\perp n_m$ appearing in the calculation of $\varphi_m^1(x,y)$ in (17) is of $O(NM)$, since $\Delta_\perp$ is a matrix with only five entries per row. The operator $\Delta_\parallel^{-2}$ is simply evaluated by applying the algorithm of (20) twice and using a correction as in (21), but with $U=0$.

Once we have calculated the potential $\varphi_m(x,y)$, the electric fields are easily obtained in $O(NM)$ by
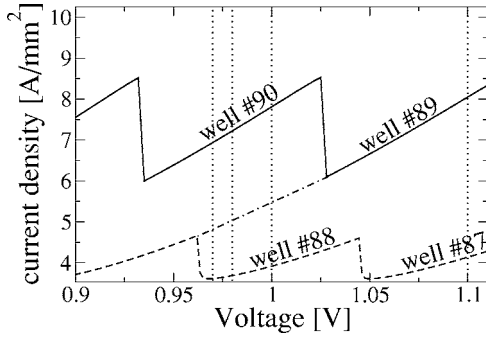
FIG. 1. Static current density vs voltage characteristic for superlattice without lateral patterns. The labels on the branches indicate the well number with the maximum charge density (domain boundary). The solid line denotes the current density during an up-sweep of the voltage from $U=0.1$ V to $U=2.0$ V, while the broken line indicates the corresponding down-sweep from $U=2.0$ V to $U=0.1$ V. The dash-dotted curve is obtained by down-sweeping the voltage from an initial condition located on the up-sweep curve at $U=1.03$ V to $U=0.96$ V. The dotted vertical lines mark the voltages considered in Figs. 2 and 3.

$$F_m^{\parallel}(x,y) = \frac{\varphi_{m+1}(x,y) - \varphi_m(x,y)}{d}, \qquad (22)$$

$$\mathbf{F}_m^{\perp}(x,y) = -\boldsymbol{\nabla}_{\perp}\varphi_m(x,y) \qquad (23)$$

and can be used in (6) and (3) to calculate the current densities needed for the electron density evolution equation (1).

IV. STABILITY OF INHOMOGENEOUS LATERAL PATTERNS

For the numerical implementation of the scheme described in Sec. III, we use a superlattice as studied in Ref. 25, i.e., a superlattice with $N=100$ periods of $b=5$ nm $Al_{0.3}Ga_{0.7}As$ barriers and $w=8$ nm GaAs quantum wells, doping $N_D=7.7\times10^{16}$ cm^{-3} and scattering induced broadening $\Gamma=8$ meV at $T=20$ K. It is typical of samples used in experiments.[26] In contrast to Ref. 25, we use a large contact conductivity $\sigma=500$ Ω^{-1} m^{-1} in order to avoid the generation of moving fronts (domains) at the emitter. For simplicity, we assume that the sample extension in the y direction is small, such that pattern formation can only occur in the x direction. We choose $L_x=50$ μm and $M=25$ discretization points. We calculate $\varphi_m(x,y)$ only to the lowest order and assume an effective diffusion constant of $D_0\approx0.01$ m^2/s.

In the homogeneous case without lateral pattern formation, the superlattice shows a stationary current-voltage characteristic with branches associated with stationary high field domains attached to the collector (Fig. 1). The branches are labeled by the number m of the well in which the peak of the electron charge distribution, i.e., the domain boundary, is located.

Due to the multistability apparent from Fig. 1, we might expect stable lateral patterns, where the superlattice is divided laterally along the x axis into regions with operating points on different branches, introducing additional lateral
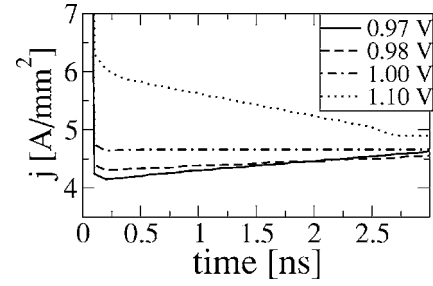
FIG. 2. Current vs time for inhomogeneous initial condition at various voltages. At $t=0$, accumulation fronts are placed in the left half of well 90 and the right half of well 88.

domain boundaries. We prepare initial conditions, with the left and right halves of the superlattice corresponding to operating points on branch numbers 90 and 88, respectively. This is achieved by putting electron accumulation fronts at the appropriate positions in wells 90 and 88. We then study the response of this initial configuration to various voltages.

The resulting current traces and electron densities are shown in Figs. 2 and 3, respectively. We see that for $U=0.97$ V the sharp current peak from the switch-on of the external voltage, pushes the accumulation front in the left half from well 90 to 89 already at $t=0.1$ ns. The current density is then given by the average of the current densities of the operating points at wells 88 and 89. Subsequently, the accumulation front at well 89 extends to the right and extrudes the accumulation front at 88, until at $t=3.5$ ns we arrive at a laterally homogeneous state with an operating point at well 89. During this process, the current density rises linearly to the value of the final operating point. For $U=0.98$ V, we observe a similar behavior, but the time until the final operating point on branch 89 is reached has approximately doubled. Note that branch 89 wins over branch 88, although according to Fig. 1, both branches are stable at this
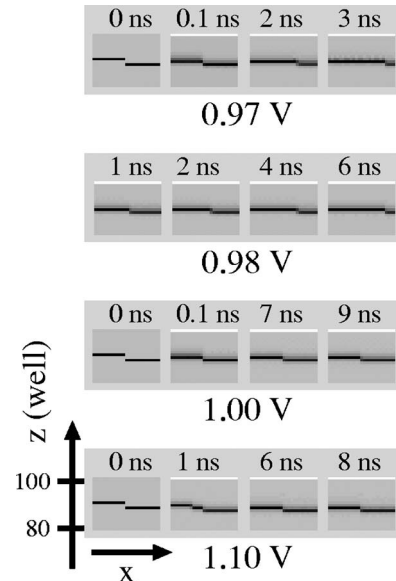
FIG. 3. Electron density evolution for inhomogeneous initial conditions as in Fig. 2, shown in the (x,z) plane of the superlattice. Dark (light) shading indicates electron accumulation (depletion).
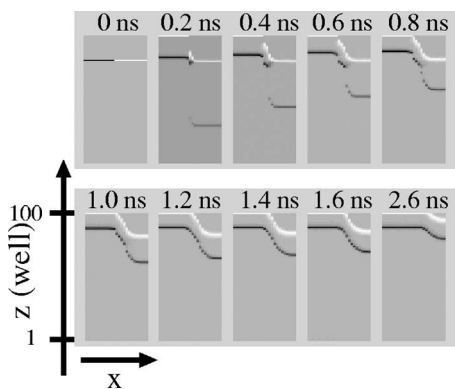
FIG. 4. Electron density evolution for inhomogeneous initial conditions with accumulation (depletion) front in left (right) half of well 80. Shaded as in Fig. 3. Bottom of each panel: emitter, top: collector.

FIG. 5. (Color online) Current vs time for the scenario in Fig. 4.

voltage. This changes for $U=1.0$ V, however, where the operating points on wells 89 and 88 coexist (Fig. 3) for longer than the simulation time, and the final current is given by the average of the currents from both branches. We, therefore, see that the stability of the mixed state depends sensitively on the applied external voltage. Qualitatively this can be understood as a change in the relative attraction (degree of stability) of the different branches with voltage. For instance at $U=0.97$ V, branch 88 is close to its instability point, as can be seen in Fig. 1. Therefore, its attraction can be expected to be lower than that of branch 89, and the transition to the final state on branch 89 is fast.

Let us finally consider the even higher voltage $U=1.1$ V, where the initial condition of the left half of the well, i.e., the accumulation front at well 90, does not correspond to a stationary state of the system (see Fig. 1). We find that the switch-on-peak shifts both accumulation fronts by two wells from wells 90 and 88 to 89 and 87, respectively, within less than 0.1ns. Then the electron accumulation from well 89 drops to well 88 starting from the middle of the sample, until at $t=7$ ns we reach a stable configuration with the left (right) half of the sample on branch 88 (87). During this transition, the current density drops linearly, as expected from the weighted average of the three involved operating points. Again this behavior can be qualitatively explained by a lack of attractiveness of branch 89 compared to branch 88, since at this voltage branch 89 is close to its upper instability point (see Fig. 1).

It is also interesting to consider an initial condition, with an accumulation front in the left half, and a depletion front in the right half of the same well. Such a configuration is shown in Fig. 4. Note that, in this case, the initial field profiles in the two halves of the superlattice are very different. While in the
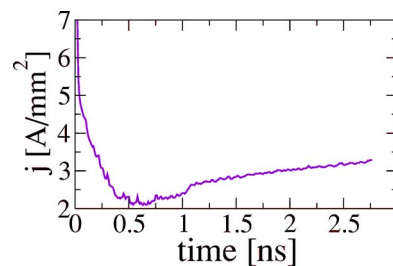
left half, the high field domain is located at the collector as before, the depletion front in the right half induces a high field domain at the emitter. To meet the overall constant voltage condition (8), this high field domain is compensated by a domain of initially negative fields at the collector. We see that a new accumulation front is generated at the emitter in the right half of the sample and moves toward the collector. Together with the already present fronts, we thus obtain a dipole (depletion + accumulation front) in the right, and a monopole (accumulation front) in the left part of the sample. As the dipole moves toward the collector, the monopole extends toward the right, until it eventually occupies the whole sample width. This behavior is also reflected by the corresponding current trace (cf. Fig. 5), which for $t > 1.0$ ns can be explained as the weighted average of the dipole current j_d and the current of the final operating point.

V. CONCLUSIONS

In conclusion, we have developed a theoretical framework which describes the combined lateral and vertical electron density dynamics in a weakly coupled superlattice and have proposed an efficient scheme for solving the resulting dynamical equations. We have seen that even in a superlattice without self-sustained oscillations, the inclusion of lateral degrees of freedom leads to qualitatively different effects such as stable mixed states where a high field and a low field domain coexist within the same well. This reveals aspects of front interaction processes, which are fundamentally different from the one-dimensional vertical interaction scenarios studied for instance in Ref. 13. These effects might be of relevance for dynamic switching and relocation of domain boundaries under voltage sweep in superlattices with large lateral extensions.

ACKNOWLEDGMENT

*Present address: Tyndall National Institute, Lee Maltings, Cork, Ireland.

[1] L. Esaki and R. Tsu, IBM J. Res. Dev. **14**, 61 (1970).

[2] L. Esaki and L. L. Chang, Phys. Rev. Lett. **33**, 495 (1974).

[3] H. T. Grahn, K. von Klitzing, K. Ploog, and G. H. Döhler, Phys. Rev. B **43**, 12094 (1991).

[4] J. Kastrup, H. T. Grahn, K. Ploog, F. Prengel, A. Wacker, and E. Schöll, Appl. Phys. Lett. **65**, 1808 (1994).

[5] Y. A. Mityagin, V. N. Murzin, Y. A. Efimov, and G. K. Rasulova, Appl. Phys. Lett. **70**, 3008 (1997).

[6] M. Büttiker and H. Thomas, Phys. Rev. Lett. **38**, 78 (1977).

[7] J. Kastrup, R. Klann, H. T. Grahn, K. Ploog, L. L. Bonilla, J. Galán, M. Kindelan, M. Moscoso, and R. Merlin, Phys. Rev. B **52**, 13761 (1995).

[8] K. Hofbeck, J. Grenzer, E. Schomburg, A. A. Ignatov, K. F. Renk, D. G. Pavel'ev, Y. Koschurinov, B. Melzer, S. Ivanov, S. Schaposchnikov, and P. S. Kop'ev, Phys. Lett. A **218**, 349 (1996).

[9] J. Kastrup, R. Hey, K. H. Ploog, H. T. Grahn, L. L. Bonilla, M. Kindelan, M. Moscoso, A. Wacker, and J. Galán, Phys. Rev. B **55**, 2476 (1997).

[10] M. Patra, G. Schwarz, and E. Schöll, Phys. Rev. B **57**, 1824 (1998).

[11] A. Amann, J. Schlesner, A. Wacker, and E. Schöll, Phys. Rev. B **65**, 193313 (2002).

[12] A. Amann, K. Peters, U. Parlitz, A. Wacker, and E. Schöll, Phys. Rev. Lett. **91**, 066601 (2003).

[13] A. Amann and E. Schöll, J. Stat. Phys. **119**, 1069 (2005).

[14] E. Schöll, *Nonlinear Spatio-Temporal Dynamics and Chaos in Semiconductors* (Cambridge University Press, Cambridge, UK, 2001).

[15] A. Wacker, Phys. Rep. **357**, 1 (2002).

[16] L. L. Bonilla, J. Phys.: Condens. Matter **14**, R341 (2002).

[17] L. L. Bonilla and H. T. Grahn, Rep. Prog. Phys. **68**, 577 (2005).

[18] A. Amann, A. Wacker, L. L. Bonilla, and E. Schöll, Phys. Rev. E **63**, 066207 (2001).

[19] M. Rogozia, S. W. Teitsworth, H. T. Grahn, and K. H. Ploog, Phys. Rev. B **65**, 205303 (2002).

[20] P. T. Landsberg, *Recombination in Semiconductors* (Cambridge University Press, Cambridge, UK, 1991).

[21] V. Cheianov, P. Rodin, and E. Schöll, Phys. Rev. B **62**, 9966 (2000).

[22] M. Meixner, P. Rodin, E. Schöll, and A. Wacker, Eur. Phys. J. B **13**, 157 (2000).

[23] P. Rodin and E. Schöll, J. Appl. Phys. **93**, 6347 (2003).

[24] P. Rodin and E. Schöll, Phys. Rev. B **71**, 047301 (2005).

[25] A. Amann, A. Wacker, and E. Schöll, Physica B **314**, 404 (2002).

[26] S. Zeuner, S. J. Allen, K. D. Maranowski, and A. C. Gossard, Appl. Phys. Lett. **69**, 2689 (1996).